Shiba states in systems with density of states singularities

Surajit Basak [*] and Andrzej Ptok [†]

Institute of Nuclear Physics, Polish Academy of Sciences, W. E. Radzikowskiego 152, PL-31342 Kraków, Poland

Magnetic impurities placed in the superconductor can lead to the emergence of Yu-Shiba-Rusinov bound states. Coupling between the impurity and the substrate depends on the density of states (DOS) at the Fermi level and can be tuned by DOS singularities. In this paper, we study the role of DOS singularities using the real space Bogoliubov–de Gennes equations for chosen lattice models. To uncover the role of these singularities (Dirac point, van Hove singularity, or the flat band), we study honeycomb, kagome, and Lieb lattices. We show that the properties of the Shiba state strongly depend on the type of lattice. Nevertheless some behaviors are generic, e.g., dependence of the critical magnetic coupling on the DOS at the Fermi level. However, the Shiba states realized in the Lieb lattice exhibit extraordinary properties, which can be explained by the presence of a few nonequivalent sublattices. Depending on the location of the magnetic impurity in the chosen sublattice, the value of critical magnetic coupling J_c can be reduced or enhanced when the flat band is located at the Fermi level. In this context, we also present differences in the local DOS and coherence lengths for different sublattices in the Lieb lattice.

I. INTRODUCTION

The interplay between a superconducting system and magnetic impurity can lead to the emergence of Yu-Shiba-Rusinov (YSR) bound states [1–3] (the Shiba states for short), due to local breaking of the Cooper pairs by the magnetic moment of the impurity [Fig. 1(a)]. This leads to the formation of in-gap states inside the superconducting gap, with spatially oscillating wave function [4]. Recent progress in the experimental techniques has resulted in increased experimental [5] as well as theoretical [6] attention in this field.

Dimensionality of the system plays a critical role in the formation of the Shiba state. The three-dimensional conventional superconductor shows a fast decay of the YSR states away from the magnetic impurity. Contrary to this, in the case of two-dimensional systems the YSR states are characterized by the long-range coherence length [7,8].

The YSR states can be observed experimentally within the topographic scanning tunneling microscopic (STM) imaging of the surface. It was first reported in the presence of Mn and Gd adatoms on the surface of a single-crystal Nb sample [9]. Increased resolution allows mapping of the YSR states occurring from individual orbitals of the atom. Such cases have been reported in transition metal atoms deposited on conventional superconductors (Pb [10–14] or Nb [15–18]). YSR states were also realized by depositing Fe on the NbSe$_2$ surface [7,19–21]. Similar observations can be made in the presence of magnetic molecules, such as (Mn, Cu, V, or Co) phthalocyanine [14,22–28] or (Fe or Mn) porphyrin [29–31]. Also, recently the fabrication of YSR states in the iron-based

unconventional superconductor attracted a lot of attention [32–34].

The presence of artificial structures of magnetic atoms can lead to the emergence of in-gap Shiba bands. If the nontrivial topological phase is realized [35], the Majorana end modes can occur [36]. Recently this type of structures were realized in many experiments [37–43].

Motivation. In the simplest case, the magnetic impurity gives rise to a pair of in-gap states, symmetric in energy with respect to the Fermi level, characterized as YSR states. For the classical spin, the energies of the in-gap YSR states are given as

$$E_{\mathrm{YSR}} = \pm \Delta \frac{1 - \alpha^2}{1 + \alpha^2}, \qquad (1)$$

where $\alpha^2 = \pi N(E_F)J$ is the dimensionless impurity coupling (neglecting Coulomb scattering), Δ is the superconducting gap, $N(E_F)$ denotes the density of states (DOS) at the Fermi level E_F, while J describes coupling between magnetic moment and electrons. At $J = J_c$ the YSR states cross the Fermi level [$E_{\mathrm{YSR}}(J_c) = 0$]. That point is related to the quantum phase transition (QPT), also known as the 0-π transition. During the QPT, the ground state is changed from the BCS-type spinless state (for the weak coupling $J < J_c$) to the singly occupied (spinful configuration (for strong coupling $J > J_c$) [44]. As we can see from Eq. (1), the value of J_c is proportional to $1/N(E_F)$. Indeed, previous study of the YSR states in the presence of the van Hove singularity (VHS) show that the tuning of $N(E_F)$ by the VHS can lead to enhanced J_c [45]. A similar observation was reported in the case of the critical temperature of the *s-wave* and *d-wave* superconductors on a square lattice, where it was shown that T_c can be tuned by increasing $N(E_F)$ [46]. Similarly for the hexagonal lattice,

---

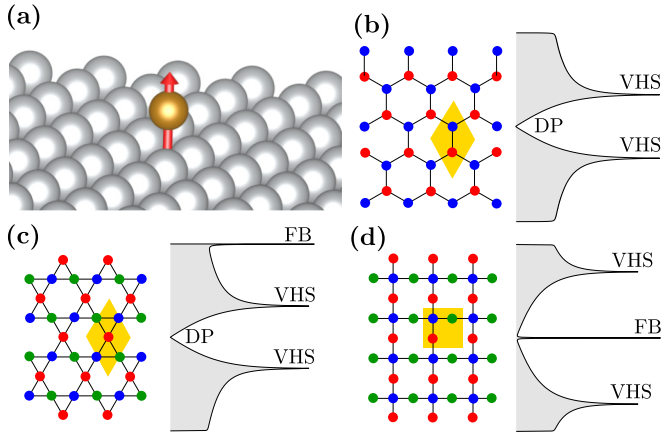[*]surajit.basak@ifj.edu.pl
[†]aptok@mmj.pl

FIG. 1. (a) Schematic representation of the magnetic atom (brown ball) deposited on the superconducting surface (silver balls). Studies performed on two-dimensional lattices and their density of states: (b) hexagonal, (c) kagome, and (d) Lieb lattices. The colors of the dots (red, green, or blue) denote nonequivalent sites, while the yellow quadrangle marks the primitive unit cell. In the case of a hexagonal and a kagome lattice, the Dirac point (DP) is realized. The flat bands (FBs) are observed in the Lieb and kagome lattices. The saddle points in the band structures give rise to van Hove singularities (VHSs) in all lattices.

in the presence of the magnetic field, the VHS can lead to superconductivity reentrant behavior [47].

General behavior of the in-gap energies is well known from the milestone works of Yu, Shiba, and Rusinov [1–3]. The general J dependence of the bound state (in-gap) energies is given by Eq. (1). Similar behavior is observed also in the presence of several atoms, e.g., monoatomic chains [48,49], where in-gap states cross the Fermi level a few times. Moreover, this type of behavior of the in-gap state energies was observed experimentally in the case of a magnetic molecule of manganese phthalocyanine (MnPc) on a Pb(111) surface [23].

Another aspect of the Shiba states is strongly associated with the Fermi surface of the studied system [50]. Interestingly, the pattern of the localized state induced by the magnetic impurity reflects some properties of the Fermi surface of the system [51]. This is well visible in the star-shaped localization of the Shiba states around the magnetic impurity on a NbSe$_2$ [7] or La [8] surface, which is associated with a sixfold symmetry of the Fermi surface of these systems.

In this paper we study the role of DOS singularities on the YSR states using exact lattice models [Figs. 1(b)–1(d)]. These techniques allow us to study not only VHS [realized, e.g., in the honeycomb lattice [Fig. 1(b)], but also the role of flat bands [realized, e.g., in a kagome or Lieb lattice [52], presented in Figs. 1(c) and 1(d), respectively]. The flat bands can play an important role in the context of the recently discovered superconducting kagome systems (such as AV$_3$Sb$_5$ [53] or LaRu$_3$Si$_2$ [54]), artificial structures (like twisted bilayer graphene [55,56], or some type of heterostructures and interfaces [57]). Also, recent progress in the realization of artificial lattices [58] opens up a new opportunity to study the YSR states in the flat-band systems.

However, the DOS does not contain full information about the lattice, which can be important in the context of correct description of the Shiba states in real systems. As an example, this can be important in the context of the recent study of the Shiba states based on the Green's function approach [45,50]. In our study we analyze this problem, based on the real space tight-binding formulation. Our finding shows the important role played by the sublattices present in the system. Depending on the position of the magnetic impurity, the Shiba states can exhibit "extreme" behaviors, even within one specific lattice.

The paper is organized as follows. The theoretical background is presented in Sec. II. In Sec. III we present the numerical results and discussions. We conclude our study in Sec. IV.

II. THEORETICAL BACKGROUND

The system is described by the Hamiltonian

$$H = H_0 + H_{SC} + H_{imp}. \tag{2}$$

The first term describes the tight-binding model of the lattice (cf. Fig. 1):

$$H_0 = -t \sum_{\langle ij \rangle \sigma} \hat{c}_{i\sigma}^\dagger \hat{c}_{j\sigma} - \mu \sum_{i\sigma} \hat{c}_{i\sigma}^\dagger \hat{c}_{i\sigma}, \tag{3}$$

where $\hat{c}_{i\sigma}^\dagger$ ($\hat{c}_{i\sigma}$) denotes the creation (annihilation) operator an electron with spin σ at site i, t is the hopping integral between nearest neighbors $\langle i, j \rangle$, and μ is the chemical potential. The second term is responsible for superconductivity:

$$H_{SC} = \sum_i (\Delta \hat{c}_{i\uparrow}^\dagger \hat{c}_{i\downarrow}^\dagger + \text{H.c.}), \tag{4}$$

where Δ is the superconducting gap. The third term describes coupling of the magnetic impurity with the underlying lattice. In our investigation, we describe the magnetic impurity captured by H_{imp} as a classical spin aligned out of plane and only present on site [i.e., term proportional to $\delta(r_0 - r_i)$, where the subscript "0" denotes the impurity site]. In this case, the scattering potential at the position of the impurity is given as

$$H_{imp} = K(\hat{c}_{0\uparrow}^\dagger \hat{c}_{0\uparrow} + \hat{c}_{0\downarrow}^\dagger \hat{c}_{0\downarrow}) - J(\hat{c}_{0\uparrow}^\dagger \hat{c}_{0\uparrow} - \hat{c}_{0\downarrow}^\dagger \hat{c}_{0\downarrow}), \tag{5}$$

where K denotes the nonmagnetic scattering potential, while J denotes the coupling strength between the electrons and the magnetic impurity. The classical magnetic impurity limit is technically achieved by taking $S \to \infty$ (large spin), while simultaneously letting $J \to 0$ so that $JS = \text{const}$ [6]. Effectively, the classical magnetic impurity acts on the system in two ways: (i) by shifting the chemical potential (K term), which effectively leads to a modification of the number of electrons at site "0"; and (ii) by an on-site Zeeman-like magnetic field ($J \equiv JS$ term, where S is magnetic moment) [6].

The Hamiltonian (2) describing the inhomogeneous problem, can be diagonalized via the following unitary transformation:

$$\hat{c}_{i\sigma} = \sum_n (u_{in\sigma} \hat{\gamma}_{n\sigma} - \sigma v_{in\sigma}^* \hat{\gamma}_{n\bar{\sigma}}^\dagger), \tag{6}$$

where $\hat{\gamma}_n$ and $\hat{\gamma}_n^\dagger$ are quasiparticle fermionic operators, and $u_{in\sigma}$ and $v_{in\sigma}$ are the eigenvector coefficients. This leads to the
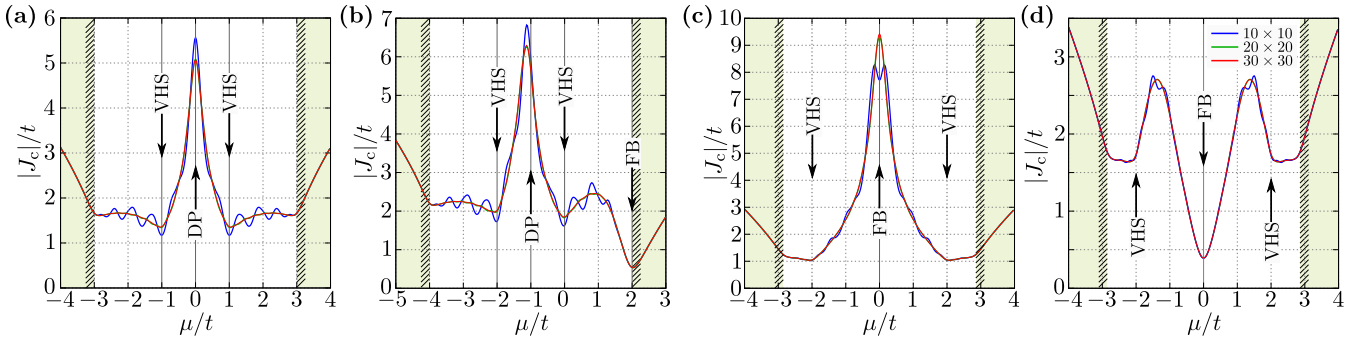
FIG. 2. Critical value of the magnetic coupling J, denoting phase transition, for different size lattices (as labeled). Results are shown for (a) hexagonal, (b) kagome, and (c),(d) Lieb lattices. For the Lieb lattice, the impurity is located at (c) the corner site or at (d) the edge site [i.e., blue and green/red sites in Fig. 1(d), respectively]. The chemical potentials for flat bands, van Hove singularities, and Dirac points, are marked as FB, VHS, and DP, respectively. Ranges of chemical potential which are out of range of the bands for given lattices are marked by green areas.

Bogoliubov–de Gennes (BdG) equations [59]:

$$\mathcal{E}_{n\sigma}\begin{pmatrix} u_{in\sigma} \\ v_{in\bar{\sigma}} \end{pmatrix} = \sum_j \begin{pmatrix} H_{ij\sigma} & D_{ij} \\ D_{ij}^* & -H_{ij\bar{\sigma}}^* \end{pmatrix}\begin{pmatrix} u_{in\sigma} \\ v_{in\bar{\sigma}} \end{pmatrix}, \quad (7)$$

where $H_{ij\sigma} = -t\delta_{\langle i,j \rangle} - [\mu + (K - \sigma J)\delta_{i0}]\delta_{ij}$ and $D_{ij} = \Delta_i \delta_{ij}$ denotes the kinetic and superconducting part of the Hamiltonian, respectively [60–62].

From the solution of the BdG equation (7) we can extract the local density of states (LDOS) for specified parameters of the system as [63]

$$\rho_i(\omega) = \sum_{n\sigma} \left[|u_{in\sigma}|^2 \delta(\omega - \mathcal{E}_{n\sigma}) + |v_{in\sigma}|^2 \delta(\omega + \mathcal{E}_{n\bar{\sigma}}) \right], \quad (8)$$

while the total DOS is given as $N(\omega) = \sum_i \rho_i(\omega)$. The LDOS for $\omega = \pm E_{\text{YSR}}$ denotes the localization of the YSR state in real space [64], and can be useful in coherence length study. In this case $\langle \rho_i(E_{\text{YSR}}) \rangle \propto \exp(-r/\zeta_c)$ denotes the wave function of the YSR states and can be used to estimate the coherence length ζ_c for a given lattice and Fermi level.

Numerical computations have been done at zero temperature $T = 0$ for the lattices with the periodic boundary conditions, containing $N_a \times N_b = 30 \times 30$ primitive unit cells. In the case of the honeycomb lattice this corresponds to 1800 sites, while for the kagome and Lieb lattices, we have 2700 sites. For simplicity and without loss of generality, we assume a constant value of $\Delta/t = 0.2$. Additionally, to study only the role of the DOS of the underlying system on the YSR states, we take $K = 0$. In numerical determination, we have replaced the Dirac δ function by the Lorentzian $\delta(\omega) = \eta/[\pi(\omega^2 + \eta^2)]$ with a small broadening $\eta = 0.05t$.

III. NUMERICAL RESULTS AND DISCUSSION

In our analysis, we consider honeycomb, kagome, and Lieb lattices. Each of them is formed by the unit cells containing more than one site, and as a consequence in the DOS a few bands can be distinguished. The honeycomb (kagome) lattice is formed by unit cells containing two (three) equivalent sites (in Fig. 1 represented by dots with different colors). In this case, one of the sublattices can be transformed to another by the combination of a few translation, rotation, or reflection

operations. Contrary to this, the Lieb lattice is formed by unit cells containing two different types of sites. Two edge sites [green/red dots in Fig. 1(c)] are equivalent to each other, but nonequivalent to the corner site (blue dots). As a result, the Lieb lattice is characterized by two nonequivalent sublattices; the sublattice of the edge site cannot be transformed to the corner site sublattice, and vice versa. We will show that this characteristic feature of the Lieb lattice plays an important role in the realization of the Shiba states.

Depending on the lattice, in the DOS we can find a few interesting features. For example, honeycomb and kagome lattices contain Dirac points (DPs) at band touching points. Similarly, in the DOS of the kagome and Lieb lattices the flat-band (FB) feature can be distinguished. Additionally, the VHSs in the form of characteristic peaks in the DOS are visible for all lattices. As we can see, the DOSs exhibit similar behaviors regardless of the chosen lattice. However, the DOS do not contain the full information about the lattice (e.g., symmetry of the system, number of neighboring sites, existence of eventual sublattices, etc.). Despite the similarities in DOSs, the strong differences are well visible in the chemical potential dependence of the critical magnetic coupling J_c (Fig. 2) and the Shiba state energies $\pm E_{\text{YSR}}$ (Fig. 3).

First, we notice that the J_c vs μ plot follows the same symmetry as the DOS (cf. Fig. 2 and Fig. 1). For honeycomb and Lieb lattices, the DOS is symmetric with respect to the center of the bandwidth (related to $\mu/t = 0$) and the same character is reflected in $J_c(\mu)$. Similarly, the asymmetric DOS of the kagome lattice is reflected in Fig. 2(b).

$J_c(\mu)$ exhibits a strong dependence on the position of the Fermi level which is related to μ (Fig. 2). However, the dependence of J_c on $N(E_F)$ is highly unexpected. In the case of honeycomb and kagome lattices [presented in Figs. 2(a) and 2(b), respectively], the presence of the DP with $N(E_F) = 0$ leads to the occurrence of a peak in J_c. Contrary to this, the presence of VHS leads to a relatively small reduction of J_c. The most important modification of J_c is introduced by the FB (theoretically with infinite DOS) in the kagome lattice. In this case, J_c decreases dramatically to its minimum value with respect to rest of the plot. Nevertheless, the most surprising results can be found in the Lieb lattice [Figs. 2(c) and 2(d)]. When impurity is located at the corner site, $J_c(\mu)$ exhibits
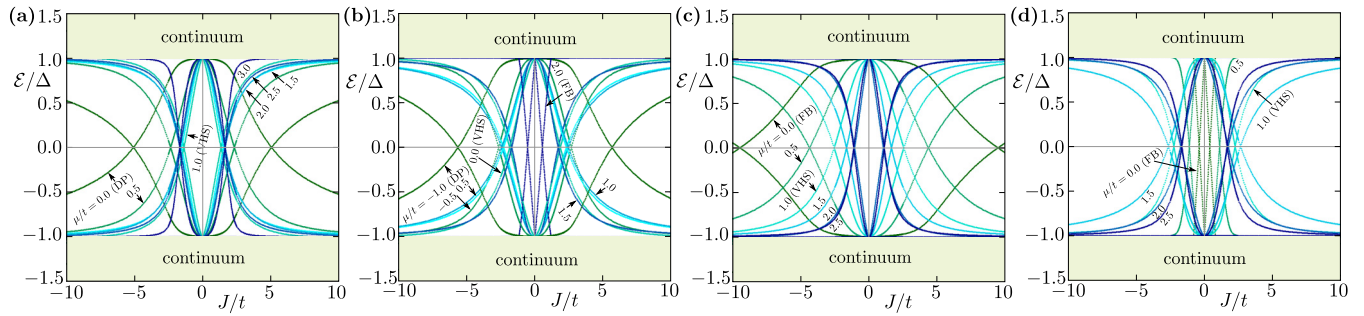
FIG. 3. In-gap spectrum of the Shiba states for different values of the chemical potential (as labeled) in the case of (a) hexagonal, (b) kagome, and (c),(d) Lieb lattices. For the Lieb lattice, the impurity was located in (c) the corner site or (d) the edge site [i.e., blue and green/red sites in Fig. 1(c), respectively]. The chemical potentials for flat bands, van Hove singularities, and Dirac points are marked as FB, VHS, and DP, respectively. Additionally, the green areas mark the ranges of energies for (out-gap) continuum states.

features similar to the honeycomb lattice [cf. Fig. 2(a) and Fig. 2(c)]. J_c reaches the maximum value when μ is located at the FB. Contrary to this, the impurity located at the edge site leads to opposite (expected) behaviors, i.e., a dramatic decrease of J_c for $\mu/t = 0$ (corresponding to the FB).

The results presented here are sensitive to the number of sites of the discussed system (cf. lines with different color in Fig. 2). Nevertheless, $J_c(\mu)$ has the same (qualitative) behavior independent of the size of the system, and describes the thermodynamic limit ($N_a \times N_b \to \infty$) relatively well for lattice with 30×30 unit cells. Similar effects can be observed with decreasing Δ, when the emergence of the superconducting phase (i.e., when Δ is comparable to the gap between states) strongly modifies states in the system.

The value of $J_c(\mu)$ is related to the Shiba state energy $\pm E_{YSR}$ (Fig. 3). The reduced value of J_c induced by VHS or FB leads to a nearly linear dependence of E_{YSR} on coupling strength J. Similar features of the Shiba states in the presence of VHS were discussed by Uldemolins *et al.* in Ref. [45]. The authors found a strong reduction of J_c when the Fermi level was located at the VHS. In this case, the linearity of $E_{YSR}(J)$ was also reported around J_c. In our case, the presence of a FB allows the existence of the Shiba state with exactly linear $E_{YSR}(J)$ dependence [cf. Fig. 3(b) or Fig. 3(d)]. For a system with small DOS (e.g., μ corresponding to the DP) or approximately constant value of DOS, the Shiba state energy has expected features, given by the general formula (1).

Extraordinary properties of the Shiba states in the Lieb lattice can be directly connected with the presence of two sublattices, formed by the corner sites or the edge sites. The partial DOS projected on the corner or edge sites, which clearly show the impact of each sublattice [58,65,66] could be a proof of this hypothesis. In particular, the whole spectral weight of the FB peak in the DOS corresponds to the edge site sublattice [giving vanishing PDOS for the corner site sublattice and opposite J_c tuning for $\mu/t = 0$; cf. Figs. 2(c) and 2(d)]. Contrary to the FB peak, the DOS at the VHS has contributions from both sublattices [66]. This very well explains the $J_c(\mu)$ dependence the for corner site sublattice [Fig. 2(c)] and the edge site sublattice [Fig. 2(d)]. A second direct proof can be given by the LDOS of the Shiba states induced by magnetic impurities located at a given sublattice (Fig. 4). As we can see, the pattern of the LDOS corresponding to the

Shiba state strongly depends on the position of the impurity (cf. top and bottom panels in Fig. 4). Similarly, the coherence length depends on the parameters of the systems (cf. left and right panels in Fig. 4). From these numerical studies we can find that the Shiba state is mostly localized at the same sublattice as the magnetic impurity site (marked by a black circle). Only in the sites which are neighbors to the impurity's location, is some modification of LDOS observed. Interestingly, similar behavior was observed experimentally within the STM measurements of the Zn impurity in the copper-dioxide Lieb lattice of the high temperature superconductor $Bi_2Sr_2CaCu_2O_{8+\delta}$ [67]. In this case, for the impurity located at the corner site, the LDOS of bound states was observed
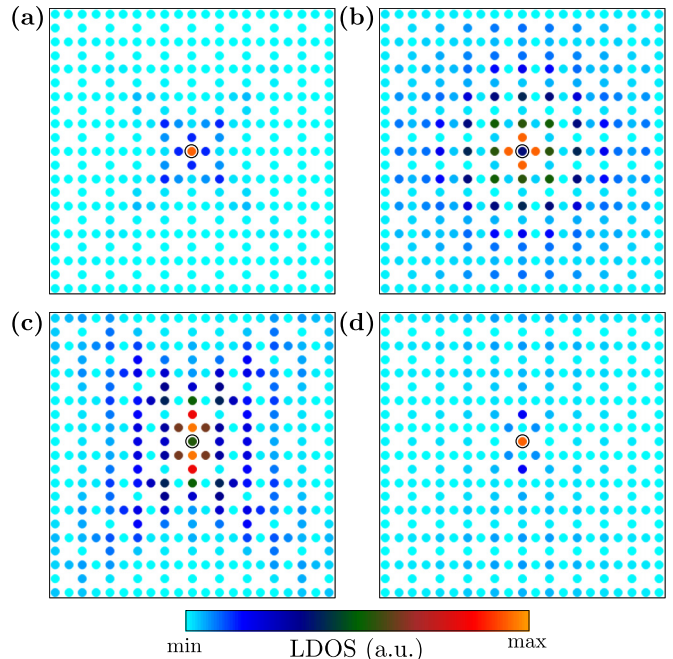

FIG. 4. Local density of states (LDOS) for the Lieb lattice. The position of the impurity is marked by a black circle. In panels (a) and (b) the impurity is located at the corner site [blue site in Fig. 1(d)], while in (c) and (d) it is located at the edge site [green or red site in Fig. 1(d)]. Results are shown for the following values of parameters $(\mu/t; J/t)$: (2.0; 0.5), (0.5; 7.5), (2.0; 5.0), and (0.5; 0.5) for panel (a), (b), (c), and (d), respectively.
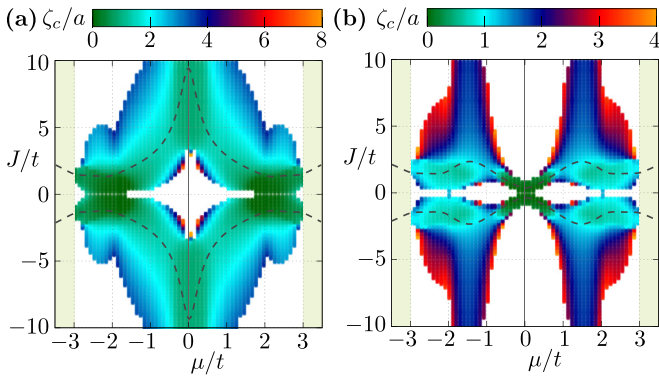
FIG. 5. Coherence length ζ_c as a function of chemical potential μ and magnetic coupling J for the Lieb lattice when the impurity is located at (a) the corner site or (b) the edge site [i.e., blue and green/red site in Fig. 1(c), respectively]. Dashed black line denotes the value of critical J for a given μ (cf. Fig. 2). Results are presented for Shiba states with energies $|E_{YSR}| < 0.95\Delta$. a is the distance between neighboring sites (i.e., distance between the corner and edge state), taken as a unit of distance.

in diagonal directions (rotated $45°$ to the x-y axis), i.e., a situation similar to Fig. 4(a).

Exponential decay of the Shiba states as a function of distance from the impurity gives information about the coherence length ζ_c (Fig. 5). Similar to J_c for the Lieb lattice, the coherence length depends on the sublattice in which the magnetic impurity is located. Moreover, around $J_c(\mu)$ (represented by the black dashed line) the coherence length is relatively small (in range $\sim 2a$ or $\sim 1a$ for impurity in the corner site or edge site, respectively). For $J \gg J_c$ the coherence length can be much bigger—this behavior is also visible in the LDOS discussed earlier (Fig. 4).

IV. SUMMARY

In this paper we discuss the effect of density of states singularities on the Shiba states. In particular, we investigated the role of Dirac point, van Hove singularity, and flat band in honeycomb, kagome, and Lieb lattices. In its simplest form, the energy of the Shiba states strongly depends on the density of states at the Fermi level. For example, the presence of a flat band leads to strong suppression of the critical magnetic coupling J_c, while the existence of the Dirac point leads to an enhanced J_c. We examined the tuning of the parameters (e.g., energy or critical magnetic coupling) describing the Shiba states in the aforementioned lattices.

The Shiba states realized in the honeycomb and the kagome lattices exhibit typical behaviors. For the Fermi level at the Dirac point we observed a maximum of J_c, while the flat band strongly suppresses J_c. Similarly, the van Hove singularity leads to a decrease in J_c. Contrary to this, the Lieb lattice containing two sublattices (of the corner and edge sites), exhibits extraordinary behavior. In this case, the properties of the Shiba states strongly depend on the position of the magnetic impurity (in a specific sublattice). The atypical behavior is observed in J_c, the local density of states, and coherence length studies. (i) The magnetic coupling exhibits dependence similar to the density of states projected on the specific sublattice. (ii) The majority of the spectral weight in the local density of states of the Shiba states is observed in the sublattice containing the magnetic impurity. (iii) The coherence length strongly depends on the sublattice in which the magnetic impurity is located. These findings should be generic for systems with a few sublattices, and can explain some experimental data observed in systems where a Lieb lattice is realized (like high temperature superconductors).

[1] L. Yu, Bound state in superconductors with paramagnetic impurities, Acta Phys. Sin. **21**, 75 (1965).

[2] H. Shiba, Classical spins in superconductors, Prog. Theor. Exp. Phys. **40**, 435 (1968).

[3] A. I. Rusinov, Theory of gapless superconductivity in alloys with paramagnetic impurities, Zh. Eksp. Theor. Fiz. **57**, 2047 (1969).

[4] A. L. Fetter, Spherical Impurity in an Infinite Superconductor, Phys. Rev. **140**, A1921 (1965).

[5] B. W. Heinrich, J. I. Pascual, and K. J. Franke, Single magnetic adsorbates on s-wave superconductors, Prog. Surf. Sci. **93**, 1 (2018).

[6] A. V. Balatsky, I. Vekhter, and J.-X. Zhu, Impurity-induced states in conventional and unconventional superconductors, Rev. Mod. Phys. **78**, 373 (2006).

[7] G. C. Ménard, S. Guissart, C. Brun, S. Pons, V. S. Stolyarov, F. Debontridder, M. V. Leclerc, E. Janod, L. Cario, D. Roditchev,

P. Simon, and T. Cren, Coherent long-range magnetic bound states in a superconductor, Nat. Phys. **11**, 1013 (2015).

[8] H. Kim, L. Rózsa, D. Schreyer, E. Simon, and R. Wiesendanger, Long-range focusing of magnetic bound states in superconducting lanthanum, Nat. Commun. **11**, 4573 (2020).

[9] A. Yazdani, B. A. Jones, C. P. Lutz, M. F. Crommie, and D. M. Eigler, Probing the local effects of magnetic impurities on superconductivity, Science **275**, 1767 (1997).

[10] S.-H. Ji, T. Zhang, Y.-S. Fu, X. Chen, X.-C. Ma, J. Li, W.-H. Duan, J.-F. Jia, and Q.-K. Xue, High-Resolution Scanning Tunneling Spectroscopy of Magnetic Impurity Induced Bound States in the Superconducting Gap of Pb Thin Films, Phys. Rev. Lett. **100**, 226801 (2008).

[11] M. Ruby, F. Pientka, Y. Peng, F. von Oppen, B. W. Heinrich, and K. J. Franke, Tunneling Processes Into Localized Subgap States in Superconductors, Phys. Rev. Lett. **115**, 087001 (2015).

[12] M. Ruby, Y. Peng, F. von Oppen, B. W. Heinrich, and K. J. Franke, Orbital Picture of Yu-Shiba-Rusinov Multiplets, Phys. Rev. Lett. **117**, 186801 (2016).

[13] D.-J. Choi, C. Rubio-Verdú, J. de Bruijckere, M. M. Ugeda, N. Lorente, and J. I. Pascual, Mapping the orbital structure of impurity bound states in a superconductor, Nat. Commun. **8**, 15175 (2017).

[14] S. Y. Song, Y. S. Park, Y. Jeong, M.-S. Kim, K.-S. Kim, and J. Seo, Yu-Shiba-Rusinov bound states studied by tuning the electron density at the fermi energy, Phys. Rev. B **103**, 214509 (2021).

[15] A. Odobesko, D. Di Sante, A. Kowalski, S. Wilfert, F. Friedrich, R. Thomale, G. Sangiovanni, and M. Bode, Observation of tunable single-atom Yu-Shiba-Rusinov states, Phys. Rev. B **102**, 174504 (2020).

[16] F. Küster, S. Brinker, S. Lounis, S. S. P. Parkin, and P. Sessi, Long range and highly tunable interaction between local spins coupled to a superconducting condensate, Nat. Commun. **12**, 6722 (2021).

[17] F. Friedrich, R. Boshuis, M. Bode, and A. Odobesko, Coupling of Yu-Shiba-Rusinov states in one-dimensional chains of Fe atoms on Nb(110), Phys. Rev. B **103**, 235437 (2021).

[18] P. Beck, L. Schneider, L. Rózsa, K. Palotás, A. Lászlóffy, L. Szunyogh, J. Wiebe, and R. Wiesendanger, Spin-orbit coupling induced splitting of Yu-Shiba-Rusinov states in antiferromagnetic dimers, Nat. Commun. **12**, 2040 (2021).

[19] J. Senkpiel, C. Rubio-Verdú, M. Etzkorn, R. Drost, L. M. Schoop, S. Dambach, C. Padurariu, B. Kubala, J. Ankerhold, C. R. Ast, and K. Kern, Robustness of Yu-shiba-Rusinov resonances in the presence of a complex superconducting order parameter, Phys. Rev. B **100**, 014502 (2019).

[20] E. Liebhaber, S. Acero González, R. Baba, G. Reecht, B. W. Heinrich, S. Rohlf, K. Rossnagel, F. von Oppen, and K. J. Franke, Yu–Shiba–Rusinov states in the charge-density modulated superconductor NbSe$_2$, Nano Lett. **20**, 339 (2020).

[21] X. Yang, Y. Yuan, Y. Peng, E. Minamitani, L. Peng, J.-J. Xian, W.-H. Zhang, and Y.-S. Fu, Observation of short-range Yu–Shiba–Rusinov states with threefold symmetry in layered superconductor 2H-NbSe$_2$, Nanoscale **12**, 8174 (2020).

[22] K. J. Franke, G. Schulze, and J. I. Pascual, Competition of superconducting phenomena and Kondo screening at the nanoscale, Science **332**, 940 (2011).

[23] N. Hatter, B. W. Heinrich, M. Ruby, J. I. Pascual, and K. J. Franke, Magnetic anisotropy in Shiba bound states across a quantum phase transition, Nat. Commun. **6**, 8988 (2015).

[24] M. Etzkorn, M. Eltschka, B. Jäck, C. R. Ast, and K. Kern, Mapping of Yu-Shiba-Rusinov states from an extended scatterer, arXiv:1807.00646.

[25] L. Malavolti, M. Briganti, M. Hänze, G. Serrano, I. Cimatti, G. McMurtrie, E. Otero, P. Ohresser, F. Totti, M. Mannini, R. Sessoli, and S. Loth, Tunable spin–superconductor coupling of spin 1/2 vanadyl phthalocyanine molecules, Nano Lett. **18**, 7955 (2018).

[26] J. Brand, S. Gozdzik, N. Néel, J. L. Lado, J. Fernández-Rossier, and J. Kröger, Electron and Cooper-pair transport across a single magnetic molecule explored with a scanning tunneling microscope, Phys. Rev. B **97**, 195429 (2018).

[27] S. Kezilebieke, M. Dvorak, T. Ojanen, and P. Liljeroth, Coupled Yu–Shiba–Rusinov states in molecular dimers on NbSe$_2$, Nano Lett. **18**, 2311 (2018).

[28] S. Kezilebieke, R. Žitko, M. Dvorak, T. Ojanen, and P. Liljeroth, Observation of coexistence of Yu-Shiba-Rusinov states and spin-flip excitations, Nano Lett. **19**, 4614 (2019).

[29] N. Hatter, B. W. Heinrich, D. Rolf, and K. J. Franke, Scaling of Yu-Shiba-Rusinov energies in the weak-coupling Kondo regime, Nat. Commun. **8**, 2016 (2017).

[30] L. Farinacci, G. Ahmadi, M. Ruby, G. Reecht, B. W. Heinrich, C. Czekelius, F. von Oppen, and K. J. Franke, Interfering Tunneling Paths Through Magnetic Molecules on Superconductors: Asymmetries of Kondo and Yu-Shiba-Rusinov Resonances, Phys. Rev. Lett. **125**, 256805 (2020).

[31] C. Rubio-Verdú, J. Zaldívar, R. Žitko, and J. I. Pascual, Coupled Yu-Shiba-Rusinov States Induced by a Many-Body Molecular Spin on a Superconductor, Phys. Rev. Lett. **126**, 017001 (2021).

[32] D. Wang, J. Wiebe, R. Zhong, G. Gu, and R. Wiesendanger, Spin-Polarized Yu-Shiba-Rusinov States in an Iron-Based Superconductor, Phys. Rev. Lett. **126**, 076802 (2021).

[33] D. Chatzopoulos, D. Cho, K. M. Bastiaans, G. O. Steffensen, D. Bouwmeester, A. Akbari, G. Gu, J. Paaske, B. M. Andersen, and M. P. Allan, Spatially dispersing Yu-Shiba-Rusinov states in the unconventional superconductor FeTe$_{0.55}$Se$_{0.45}$, Nat. Commun. **12**, 298 (2021).

[34] S. Y. Song, J. H. J. Martiny, A. Kreisel, B. M. Andersen, and J. Seo, Visualization of Local Magnetic Moments Emerging from Impurities in Hund's Metal States of FeSe, Phys. Rev. Lett. **124**, 117001 (2020).

[35] A. Kobiałka, P. Piekarz, A. M. Oleś, and A. Ptok, First-principles study of the nontrivial topological phase in chains of 3d transition metals, Phys. Rev. B **101**, 205143 (2020).

[36] A. Y. Kitaev, Unpaired Majorana fermions in quantum wires, Phys.-Usp. **44**, 131 (2001).

[37] A. Kamlapure, L. Cornils, J. Wiebe, and R. Wiesendanger, Engineering the spin couplings in atomically crafted spin chains on an elemental superconductor, Nat. Commun. **9**, 3253 (2018).

[38] A. Kamlapure, L. Cornils, R. Žitko, M. Valentyuk, R. Mozara, S. Pradhan, J. Fransson, A. I. Lichtenstein, J. Wiebe, and R. Wiesendanger, Correlation of Yu–Shiba–Rusinov states and Kondo resonances in artificial spin arrays on an s-wave superconductor, Nano Lett. **21**, 6748 (2021).

[39] H. Ding, Y. Hu, M. T. Randeria, S. Hoffman, O. Deb, J. Klinovaja, D. Loss, and A. Yazdani, Tuning interactions between spins in a superconductor, Proc. Natl. Acad. Sci. USA **118**, e2024837118 (2021).

[40] E. Liebhaber, L. M. Rütten, G. Reecht, J. F. Steiner, S. Rohlf, K. Rossnagel, F. von Oppen, and K. J. Franke, Quantum spins and hybridization in artificially-constructed chains of magnetic adatoms on a superconductor, arXiv:2107.06361.

[41] L. Schneider, P. Beck, J. Neuhaus-Steinmetz, T. Posske, J. Wiebe, and R. Wiesendanger, Controlled length-dependent interaction of Majorana modes in Yu-Shiba-Rusinov chains, arXiv:2104.11503.

[42] C. Mier, J. Hwang, J. Kim, Y. Bae, F. Nabeshima, Y. Imai, A. Maeda, N. Lorente, A. Heinrich, and D.-J. Choi, Atomic manipulation of in-gap states in the β-Bi$_2$Pd superconductor, Phys. Rev. B **104**, 045406 (2021).

[43] L. Schneider, P. Beck, T. Posske, D. Crawford, E. Mascot, S. Rachel, R. Wiesendanger, and J. Wiebe, Topological Shiba bands in artificial spin chains on superconductors, Nat. Phys. **17**, 943 (2021).

[44] S. Głodzik and A. Ptok, Quantum phase transition induced by magnetic impurity, J. Supercond. Nov. Magn. **31**, 647 (2018).

[45] M. Uldemolins, A. Mesaros, and P. Simon, Effect of van Hove singularities on Shiba states in two-dimensional s-wave superconductors, Phys. Rev. B **103**, 214514 (2021).

[46] A. Ptok, K. Rodríguez, and K. J. Kapcia, Superconducting monolayer deposited on substrate: Effects of the spin-orbit coupling induced by proximity effects, Phys. Rev. Materials **2**, 024801 (2018).

[47] A. Cichy and A. Ptok, Reentrant Fulde-Ferrell-Larkin-Ovchinnikov superfluidity in the honeycomb lattice, Phys. Rev. A **97**, 053619 (2018).

[48] K. Björnson, A. V. Balatsky, and A. M. Black-Schaffer, Superconducting order parameter π-phase shift in magnetic impurity wires, Phys. Rev. B **95**, 104521 (2017).

[49] N. Mohanta, A. P. Kampf, and T. Kopp, Supercurrent as a probe for topological superconductivity in magnetic adatom chains, Phys. Rev. B **97**, 214507 (2018).

[50] J. Ortuzar, S. Trivini, M. Rouco, J. Zaldivar, J. I. Pascual, and F. S. Bergeret, Yu-Shiba-Rusinov states in 2D superconductors with arbitrary Fermi contours, arXiv:2111.02473.

[51] A. Weismann, M. Wenderoth, S. Lounis, P. Zahn, N. Quaas, R. G. Ulbrich, P. H. Dederichs, and S. Blügel, Seeing the Fermi surface in real space by nanoscale electron focusing, Science **323**, 1190 (2009).

[52] E. H. Lieb, Two Theorems on the Hubbard Model, Phys. Rev. Lett. **62**, 1201 (1989).

[53] B. R. Ortiz, L. C. Gomes, J. R. Morey, M. Winiarski, M. Bordelon, J. S. Mangum, I. W. H. Oswald, J. A. Rodriguez-Rivera, J. R. Neilson, S. D. Wilson, E. Ertekin, T. M. McQueen, and E. S. Toberer, New kagome prototype materials: Discovery of KV_3Sb_5, RbV_3Sb_5, and CsV_3Sb_5, Phys. Rev. Materials **3**, 094407 (2019).

[54] C. Mielke, Y. Qin, J.-X. Yin, H. Nakamura, D. Das, K. Guo, R. Khasanov, J. Chang, Z. Q. Wang, S. Jia, S. Nakatsuji, A. Amato, H. Luetkens, G. Xu, M. Z. Hasan, and Z. Guguchia, Nodeless kagome superconductivity in $LaRu_3Si_2$, Phys. Rev. Materials **5**, 034803 (2021).

[55] Y. Cao, V. Fatemi, S. Fang, K. Watanabe, T. Taniguchi, E. Kaxiras, and P. Jarillo-Herrero, Unconventional superconductivity in magic-angle graphene superlattices, Nature (London) **556**, 43 (2018).

[56] M. Yankowitz, S. Chen, H. Polshyn, Y. Zhang, K. Watanabe, T. Taniguchi, D. Graf, A. F. Young, and C. R. Dean, Tuning superconductivity in twisted bilayer graphene, Science **363**, 1059 (2019).

[57] T. Yilmaz, X. Tong, Z. Dai, J. T. Sadowski, E. F. Schwier, K. Shimada, S. Hwang, K. Kisslinger, K. Kaznatcheev, E. Vescovo, and B. Sinkovic, Emergent flat band electronic structure in a VSe_2/Bi_2Se_3 heterostructure, Commun. Mater. **2**, 11 (2021).

[58] M. R. Slot, T. S. Gardenier, P. H. Jacobse, G. C. P. van Miert, S. N. Kempkes, S. J. M. Zevenhuizen, C. M. Smith, D. Vanmaekelbergh, and I. Swart, Experimental realization and characterization of an electronic Lieb lattice, Nat. Phys. **13**, 672 (2017).

[59] P. G. de Gennes, *Superconductivity of Metals and Alloys* (Addison-Wesley, Reading, MA, 1989).

[60] A. Ptok, The Fulde–Ferrell–Larkin–Ovchinnikov superconductivity in disordered systems, Acta Phys. Pol. A **118**, 420 (2010).

[61] A. Ptok, The Fulde–Ferrell–Larkin–Ovchinnikov state in quantum rings, J. Supercond. Novel Magn. **25**, 1843 (2012).

[62] A. Ptok and K. J. Kapcia, Probe-type of superconductivity by impurity in materials with short coherence length: the s-wave and η-wave phases study, Supercond. Sci. Technol. **28**, 045022 (2015).

[63] H. Matsui, T. Sato, T. Takahashi, S.-C. Wang, H.-B. Yang, H. Ding, T. Fujii, T. Watanabe, and A. Matsuda, BCS-Like Bogoliubov Quasiparticles in High-T_c Superconductors Observed by Angle-Resolved Photoemission Spectroscopy, Phys. Rev. Lett. **90**, 217002 (2003).

[64] A. Ptok, S. Głodzik, and T. Domański, Yu–Shiba–Rusinov states of impurities in a triangular lattice of $NbSe_2$ with spin-orbit coupling, Phys. Rev. B **96**, 184425 (2017).

[65] W. Jiang, H. Huang, and F. Liu, A Lieb-like lattice in a covalent-organic framework and its Stoner ferromagnetism, Nat. Commun. **10**, 2207 (2019).

[66] B. Cui, X. Zheng, J. Wang, D. Liu, S. Xie, and B. Huang, Realization of Lieb lattice in covalent-organic frameworks with tunable topology and magnetism, Nat. Commun. **11**, 66 (2020).

[67] S. H. Pan, E. W. Hudson, K. M. Lang, H. Eisaki, S. Uchida, and J. C. Davis, Imaging the effects of individual zinc impurity atoms on superconductivity in $Bi_2Sr_2CaCu_2O_{8+\delta}$, Nature (London) **403**, 746 (2000).